THE JOURNAL OF PHYSICAL CHEMISTRY LETTERS
A JOURNAL OF THE AMERICAN CHEMICAL SOCIETY

pubs.acs.org/JPCL Letter

Quantum Simulation of Polarized Light-Induced Electron Transfer with a Trapped-Ion Qutrit System

Ke Sun,* Chao Fang, Mingyu Kang, Zhendian Zhang, Peng Zhang, David N. Beratan, Kenneth R. Brown, and Jungsang Kim*

Cite This: J. Phys. Chem. Lett. 2023, 14, 6071−6077 Read Online

ACCESS | Metrics & More | Article Recommendations | Supporting Information

ABSTRACT: Electron transfer within and between molecules is crucial in chemistry, biochemistry, and energy science. This study describes a quantum simulation method that explores the influence of light polarization on electron transfer between two molecules. By implementing precise and coherent control among the quantum states of trapped atomic ions, we can induce quantum dynamics that mimic the electron-transfer dynamics in molecules. We use three-level systems (qutrits), rather than traditional two-level systems (qubits), to enhance the simulation efficiency and realize high-fidelity simulations of electron-transfer dynamics. We treat the quantum interference between the electron coupling pathways from a donor with two degenerate excited states to an acceptor and analyze the transfer efficiency. We also examine the potential error sources that enter the quantum simulations. The trapped-ion systems have favorable scalings with system size compared to those of classical computers, promising access to richer electron-transfer simulations.

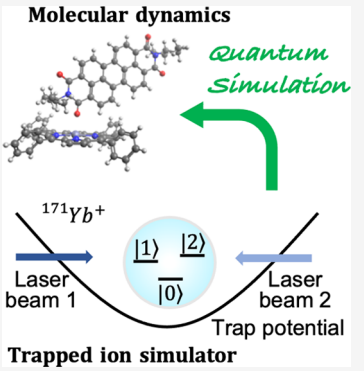

Electron transfer between molecules is of central interest in energy science, signal transduction, and catalysis in both living and nonliving systems.[1,2] Quantum effects, especially those associated with electronic coupling pathways, play a key role in the dynamics and efficiency of these reactions.[3] Light-induced electron transfer that involves many electronic and vibronic pathways can be influenced by the intensity and polarization of the excitation light.[4] Specifically, light polarization determines the superposition of the initial prepared state, and the dynamics of electron transfer are affected by the coupling interactions mediated by interfering pathways.[5,6]

Isolating and manipulating the effects of light polarization on molecular electron transfer in experiments are challenging because of the complexity of assembling and manipulating the pathways and also because of the dephasing interactions induced by the surroundings. Therefore, there have been limited experimental investigations in condensed-phase chemistry that directly manipulate the multipathway interference effects, and simulations are widely used to study quantum dynamics. Trapped-ion quantum simulators are proposed to offer an advantage over classical digital simulations for issues encountered in quantum chemistry, because computational resources that are intrinsically quantum mechanical in nature may be best suited for exploring quantum properties. Feynman first suggested the concept of quantum simulation in 1982, highlighting the potential for one quantum system to simulate another more efficiently than might be possible using classical computers.[7] Prior simulations of molecular quantum dynamics using trapped ions involved simulating quantum transport in a long ion chain by engineering coupling strengths based on inter-ion distances[8] and simulating vibrationally assisted energy transfer with qubits (two-level systems) and their collective motional modes.[9]

In this Letter, we describe a quantum simulation that uses a fully programmable trapped-ion qutrit (three-level system) platform to simulate light-induced electron-transfer dynamics. We employ a Trotterization method[10,11] that enables quantum simulation of (both time-independent and -dependent) Hamiltonians consisting of multiple noncommuting terms with high accuracy (see Experimental Methods for details).

To optimize the efficiency and accuracy of a quantum simulation task, it is preferable to minimize the number of qubits and multiqubit entangling operations employed. The latter is of particular significance due to the susceptibility of entangling operations to decoherence.[12] A potential strategy for overcoming this limitation is to use many (d) atomic levels per ion, or qu*d*its, when encoding the molecular Hamiltonian in the trapped-ion system,[13−16] to reduce the lower bound on the number of ions required to simulate an n-site (n-level) electron-transfer process from $\lceil \log_2(n) \rceil$ (qubits) to $\lceil \log_d(n) \rceil$ (qudits).[a] Here, we use a qutrit ($d = 3$) system rather than more familiar qubit ($d = 2$) structures. By using single-qutrit operations rather than two-qubit operations, we minimize the

Received: April 28, 2023
Accepted: June 20, 2023
Published: June 26, 2023

https://doi.org/10.1021/acs.jpclett.3c01166
J. Phys. Chem. Lett. 2023, 14, 6071−6077

number of ions that is required for the computation, and we replace the multi-ion entangling operations with operations that manipulate the atomic levels of a single ion. This produces significantly faster operations, with a longer coherence time and higher accuracy for tracking the electron-transfer dynamics being modeled (see the Supporting Information for a detailed comparison between qubit and qutrit simulators). The advantages of our approach are demonstrated experimentally and analyzed using classical numerical simulations, as well.

The model for electron transfer driven by polarized light (PLET) considered here contains donor and acceptor molecules, where the electron localizes. An excitation source with adjustable polarization drives a donor-localized excitation from ground state $|G\rangle$ to two degenerate or near-degenerate excited states ($|D_1\rangle$ and $|D_2\rangle$). The electronic transitions to excited states $|D_1\rangle$ and $|D_2\rangle$ are assumed to have orthogonal transition dipole moments ($\vec{\mu}_1 \perp \vec{\mu}_2$). Thus, the polarization of the excited light will determine the amplitude and phase of the excited state superposition. The interaction between the donor excited states and the acceptor state ($|A\rangle$) is described by couplings V_1 and V_2.

Electron transfer proceeds as follows (Figure 1a). Exciting light impinges on the donor−acceptor (DA) system from time

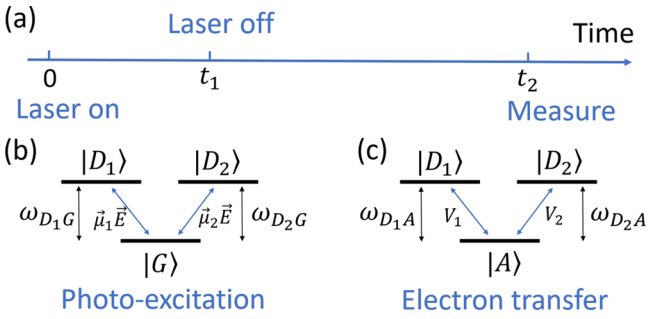

Figure 1. (a) Schematic representation of the polarized light-driven electron transfer. (b and c) Energy level diagrams indicating the ground state, degenerate donor excited states, and acceptor state.

$t = 0$ to $t = t_1$ (Figure 1b). A donor excited state superposition and the propagation of the electron from the donor to the acceptor are enabled by the off-diagonal donor−acceptor couplings denoted V_1 and V_2 (Figure 1c). The time-averaged acceptor population determines the electron-transfer efficiency between t_1 and t_2.

For DA systems of interest, light-driven electron transfer is much faster than radiative or nonradiative decay to the ground state. As such, the dynamics can be separated in approximately two steps. In the photoexcitation step ($t \in [0, t_1)$) the electronic transition occurs between the ground state and degenerate excited donor states (Figure 1b), because the coupling between donor and acceptor is weak. Then, in the electron-transfer (ET) phase ($t \in [t_1, t_2]$), the electron migrates to the acceptor (Figure 1c). Because radiative and nonradiative decay to the ground state is slower than excitation or electron transfer, only three states ($|D_1\rangle$, $|D_2\rangle$, and $|A\rangle$) are relevant to the dynamics.

Writing the electric field of the polarized light source (in atomic units) as $\vec{E}(t) = [E_x(t), E_y(t), E_z(t)]$, where x (y) is the direction of $\vec{\mu}_1$ ($\vec{\mu}_2$), the Hamiltonians describing the two steps are given by

$$\hat{H}_1(t) = \sum_j \omega_j |j\rangle\langle j| + (\mu_1 E_x(t)|G\rangle\langle D_1| + \mu_2 E_y(t)|G\rangle\langle D_2| + \text{h.c.}) \quad (1)$$

$$\hat{H}_2 = \sum_j \omega_j |j\rangle\langle j| + (V_1|D_1\rangle\langle A| + V_2|D_2\rangle\langle A| + \text{h.c.}) \quad (2)$$

where $j = \{G, D_1, D_2\}$ for the photoexcitation step and $j = \{D_1, D_2, A\}$ for the ET step and ω_j is the energy for each state ($\hbar = 1$).

We first study the photoexcitation step, which is the first step of the PLET, described by Hamiltonian $\hat{H}_1(t)$ in eq 1. Specifically, we analyze the influence of the linearly polarized light on the electronic dynamics.

As transition dipole moments of the two electronic transitions are orthogonal (Figure 1b), different polarization angles will lead to different superpositions of the degenerate states in the excited state wave function. Thus, the state of the system will have the form

$$|\Psi(t)\rangle = \alpha(t)|G\rangle + \beta_1(t)|D_1\rangle + \beta_2(t)|D_2\rangle \quad (3)$$

For a linearly polarized laser, the transition dipole moment and the electric field make a constant angle θ throughout the photoexcitation process. Consequently, the ratio r between the electric dipole transition strengths from the ground state to the two degenerate excited states is real and constant with time:

$$r \equiv \frac{\mu_1 E_x(t)}{\mu_2 E_y(t)} = \frac{\mu_1 E_0 \cos(\theta)\sin(\omega t)}{\mu_2 E_0 \sin(\theta)\sin(\omega t)} = \frac{\mu_1}{\mu_2}\cot(\theta) \quad (4)$$

As a result, the ratio between the populations of the two excited states, $P(|D_1\rangle)$ and $P(|D_2\rangle)$, is fixed over time. We quantify this ratio as the normalized population difference, defined as

$$\rho \equiv \frac{P(|D_1\rangle) - P(|D_2\rangle)}{P(|D_1\rangle) + P(|D_2\rangle)} \quad (5)$$

We also define the relative phase between the two excited states as ϕ, where $e^{i\phi} \equiv \frac{\beta_2}{|\beta_2|}/\frac{\beta_1}{|\beta_1|}$. For the linearly polarized laser, r is real, so ϕ is either 0 or π.

Figure. 2a shows the normalized population difference ρ and phase ϕ as a function of incident polarization angle θ. The population difference is obtained from both numerical calculations and quantum simulation experiments. For the quantum simulation, we map $|G\rangle$, $|D_1\rangle$, and $|D_2\rangle$ to $|0\rangle$, $|1\rangle$, and $|2\rangle$, respectively, of the trapped-ion qutrit (see Experimental Methods).

We now study the electron-transfer process, which is the second step of the PLET, described by the Hamiltonian $\hat{H}_2$ in eq 2. Specifically, we study the influence of (i) the relative phase of the initial states and (ii) the energy level difference of the two excited states on the electron-transfer efficiency.

The phase difference between the two degenerate excited states of donor $|D_{1,2}\rangle$ determines whether the interference is constructive or destructive. The initial state is selected such that the populations of the two degenerate states are equal and the population of the ground state is zero:

$$|\Psi_0\rangle = \frac{1}{\sqrt{2}}(|D_1\rangle + e^{i\phi}|D_2\rangle) \quad (6)$$

https://doi.org/10.1021/acs.jpclett.3c01166
J. Phys. Chem. Lett. 2023, 14, 6071−6077

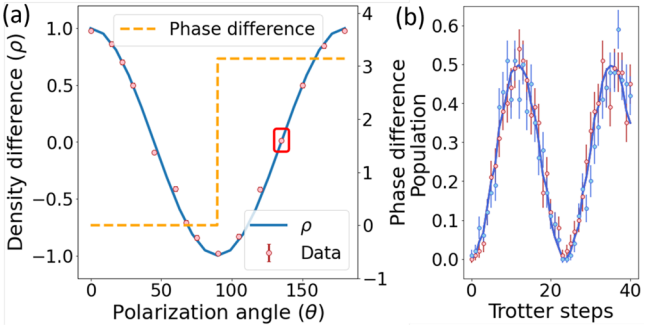

Figure 2. (a) Normalized population difference and relative phase between $|D_1\rangle$ and $|D_2\rangle$, as functions of the angle of the laser light's linear polarization. (b) Example of the raw experimental data (denoted with a red rectangular box in panel a). The red (blue) solid lines show the theoretical prediction of the population of $|D_1\rangle$ ($|D_2\rangle$), while the red (blue) points represent the experimental data. This plot shows the time evolution with $E_0 = 2.2 \times 10^9$ V/m, $\vec{\mu}_1 = e\cdot\{4.58, 0, 0\}$ a.u., and $\vec{\mu}_2 = e\cdot\{0, 4.58, 0\}$ a.u. The donor ground and excited state energies are set as $\omega_G = 0$ and $\omega_{D_1} = \omega_{D_2} = 3.89$ eV, respectively. The simulation is divided into 40 Trotter steps. Each step corresponds to an elapsed time τ of 0.198 fs. Scanning the Trotter steps is the same as observing the time evolution of electron transfer. In panel b, polarization angle θ is 135°. The populations of $|D_1\rangle$ and $|D_2\rangle$ are the same because the projections of the electric field of the laser on both electric dipole orientations of the two excited states are the same. Thus, the solid blue and red lines overlap.

This corresponds to $\alpha = 0$, $|\beta_1| = |\beta_2|$, and $\beta_2/\beta_1 = e^{i\phi}$ (see eq 3).

Figure 3 shows the results of both numerical calculations and quantum simulations describing the transfer of electrons to the acceptor state from this initial state. For the quantum simulation, we map $|A\rangle$, $|D_1\rangle$, and $|D_2\rangle$ to $|0\rangle$, $|1\rangle$, and $|2\rangle$, respectively, of the trapped-ion qutrit. Panels a and b of Figure 3 show the time-averaged values of the resulting population of the two donor states (measured as a deviation from the initial values of $|\beta_1|^2 = |\beta_2|^2 = 0.5$) and the acceptor state, respectively, as a function of initial phase difference ϕ. The time-averaged deviation of the donor population is defined as

$$\sigma_{1,2} \equiv \sqrt{\frac{\sum_i^N [P_i(|D_{1,2}\rangle) - 0.5]^2}{N}} \tag{7}$$

where i represents the ith Trotterization step. Note that when $\phi = 180°$, the initial state does not transfer any population to the acceptor state due to destructive interference between the two coupling pathways from $|D_1\rangle$ and $|D_2\rangle$, and therefore, the population of the two donor states does not change. This is also reflected by the fact that the acceptor population is zero at this value. For the parameters of the Hamiltonian summarized in the figure caption, we simulated the time evolution of the two donor state populations (Figure 3c) and the acceptor state population (Figure 3d) for an initial phase difference ϕ of 90°. The horizontal axis indicates the number of Trotter steps ($\leq$70), representing the time evolution (each step corresponding to $\tau = 0.471$ fs of time evolution).

In the case of nondegenerate donor states $|D_1\rangle$ and $|D_2\rangle$, quantum interference is expected to be suppressed compared to the degenerate case in which interference is significant. To investigate this, we begin with an initial 180° phase difference that results in destructive interference and track the changes in interference as the energy degeneracy is lifted. Note that changes in the donor's conformation could break the molecule's symmetry, lifting the degeneracy of the excited states, but the coupling between these two excited states remains small because they are orthogonally polarized.

Panels a and b of Figure 4 show the time-averaged populations of the two donor states (measured as a deviation from the initial value of 0.5) and the acceptor state, respectively, as the energy ω_{D_2} of the second donor state ($|D_2\rangle$) is varied from the energy $\omega_{D_1} = 3.86$ eV of the first donor state ($|D_1\rangle$). For degenerate states ($\omega_{D_2}/\omega_{D_1} = 1$), the destructive interference keeps the donor state populations at 0.5 each and the acceptor state population at 0. As the energy degeneracy is lifted, destructive interference is suppressed, with a very narrow full width at half-maximum (fwhm) line width of ~0.73%. Panels c and d of Figure 4 show the quantum simulation from the ion trap system (dots) and calculated (lines) values of the donor and acceptor populations as a

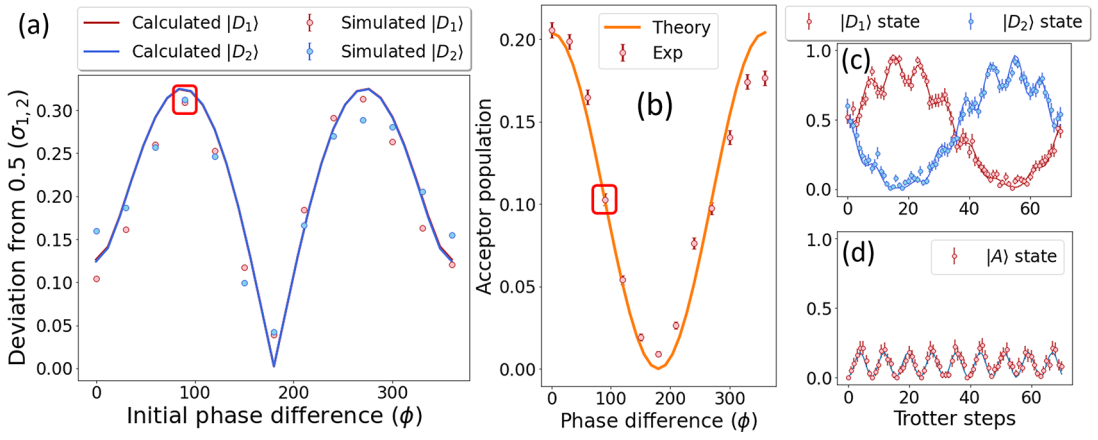

Figure 3. Simulation of electron transfer with quantum interference. The initial state is prepared as described in eq 6. (a) Simulated (dots) and calculated (lines) values of the time-averaged population of the two excited states as a function of phase difference ϕ of the initial state, plotted as the deviation from 0.5 ($\sigma_{1,2}$). (b) Time-averaged population of the acceptor state as a function of phase difference ϕ in the initial donor state. (c and d) Experimental (dots) and calculated (lines) time evolution of the two donor states and the acceptor state when $\phi = 90°$ (marked with red rectangular boxes in panels a and b). The horizontal axis corresponds to the number of Trotter steps used in the simulation, each corresponding to 0.471 fs of time evolution. Here, $\omega_{D_1} = \omega_{D_2} = 3.89$ eV, $\omega_A = 3.01$ eV, and $V_1 = V_2 = 0.25$ eV.

https://doi.org/10.1021/acs.jpclett.3c01166
J. Phys. Chem. Lett. 2023, 14, 6071−6077

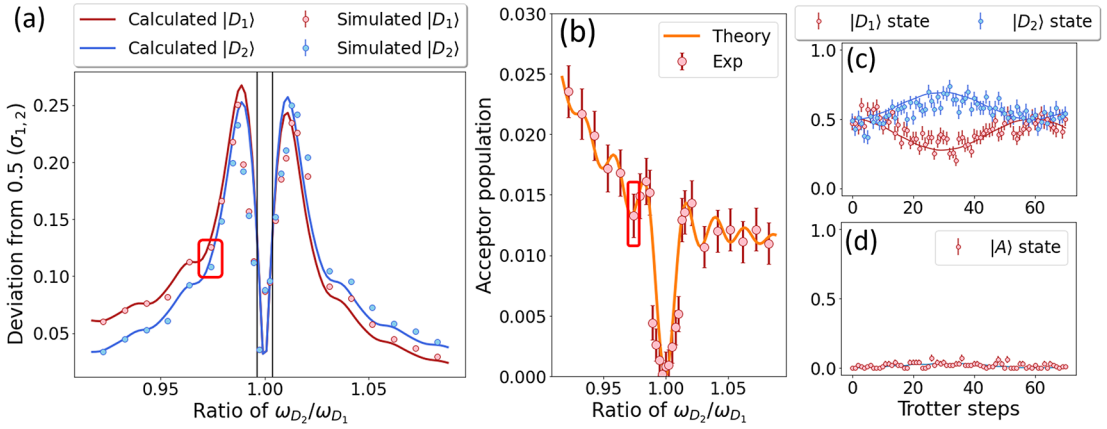

Figure 4. Simulation of destructive quantum interference (ϕ = 180°) as donor state degeneracy is lifted. (a) Simulated (dotted) and calculated (lines) values of the time-averaged population of the donor states as a function of the energy difference between the two donor states, plotted as a deviation from 0.5. (b) Time-averaged population of the corresponding acceptor state. (c and d) Simulated (dotted) and calculated (lines) time evolution of the population of the two donor states and the acceptor state, respectively, when ω_{D_2} = 3.76 and $\omega_{D_2}/\omega_{D_1}$ = 0.974 (marked with red rectangular boxes in panels a and b). The horizontal axis corresponds to ≲70 Trotter steps used in the simulation, where each step represents 0.659 fs of time evolution. Here, ω_{D_1} = 3.86 eV, ω_A = 3.01 eV, $V_1 = V_2$ = 0.25 eV, and ϕ = 180°.

function of time when $\omega_{D_2}/\omega_{D_1}$ = 0.974, plotted as a function of the number of Trotterized steps, each step corresponding to the time evolution of 0.659 fs. Although the acceptor state population is very small (<0.01), comparable to the measurement limit of our quantum simulator (determined by state preparation and measurement error), we can see clear evidence of the degradation of the destructive interference from the change in donor state populations.

We analyze the contributions of errors to the simulations to determine the accuracy of our trapped-ion quantum simulator. First, the Trotterization method used in the quantum simulation inevitably introduces errors, as the time evolution of the Hamiltonian with noncommuting terms is discretized into a finite number of steps (see eq 13). Any implementation error arising from the experimental setup adds to this theoretical Trotterization error. Therefore, we compare the theoretically predicted state populations P_{th}, derived from direct time evolution of the Hamiltonians in eqs 1 and 2, with the experimentally measured populations P_{exp} as well as the theoretical Trotterized predictions for populations P_{Tro}.

Figure 5 shows a comparison of these three quantities. Figure 5a plots the theoretical calculation of the temporal dynamics for the population of the two excited donor states, $|D_1\rangle$ and $|D_2\rangle$, during the photoexcitation step as a solid line. The solid square with dashed lines shows the calculated population using Trotterization (see eqs 13 and 15). We observe small deviations from ideal time evolution. The circular points with error bars in Figure 5a indicate the measured values from the ion trap quantum simulator, which closely follow the theoretical values within experimental error. Figure 5b shows similar comparisons for the electron-transfer step for all three states ($|D_1\rangle$, $|D_2\rangle$, and $|A\rangle$).

To analyze the deviation amoong P_{th}, P_{exp}, and P_{Tro} quantitatively, we first denote the population of state $|i\rangle$ (i = D_1, D_2, or A) at the jth Trotterization step as $P_{x,i,j}$, where x represents the ideal theoretically predicted population (x = th), the numerically predicted population using Trotterization (x = Tro), or the experimentally measured population (x = exp). We define two parameters of interest for each state $|i\rangle$: (i) the time-averaged mean distance ($\sigma_{Tro,i}$) between the population

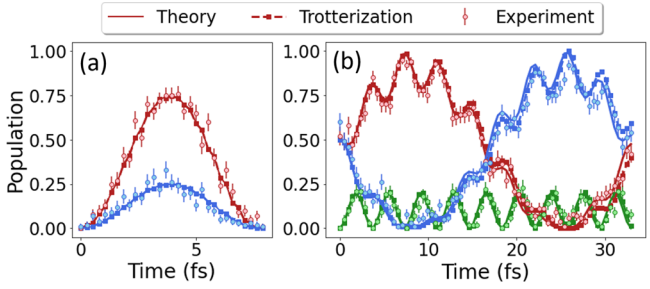

Figure 5. Comparison between the theoretically calculated populations (P_{th}, solid lines), populations predicted by the Trotterization method (P_{Tro}, dashed lines with square dots), and experimentally measured populations (P_{exp}, dots with error bars) during (a) the photoexcitation process and (b) the electron-transfer process as a function of time. In panel a, populations of both excited states $|D_1\rangle$ (red) and $|D_2\rangle$ (blue) are plotted. In panel b, populations of both excited states $|D_1\rangle$ (red) and $|D_2\rangle$ (blue) and acceptor state $|A\rangle$ (green) are plotted.

predicted by the theoretical time evolution ($P_{th,i,j}$) and the predicted population determined by Trotterization analysis ($P_{Tro,i,j}$) and (ii) the average mean distance ($\sigma_{exp,i}$) between $P_{th,i,j}$ and the experimentally measured population ($P_{exp,i,j}$). These two mean distances are defined as

$$\sigma_{Tro,i} \equiv \sqrt{\sum_{j=1}^{N} \frac{(P_{Tro,i,j} - P_{th,i,j})^2}{N}} \tag{8}$$

$$\sigma_{exp,i} \equiv \sqrt{\sum_{j=1}^{N} \frac{(P_{exp,i,j} - P_{th,i,j})^2}{N}} \tag{9}$$

where N is the number of Trotterization steps.

In both photoexcitation and electron-transfer processes, each data point in Figures 2a, 3a,b, and 4a,b is obtained by a time evolution trial. We calculate the average distance between P_{th} and P_{Tro} for each time evolution trial and obtain $\sigma_{Tro,i,k}$, where i = $|D_1\rangle$, $|D_2\rangle$, or $|A\rangle$ and k denotes the index of the time evolution trial. We then calculate the mean distance of each state $\bar{\sigma}_{Tro,i}$ versus the theoretical value by averaging over k.

https://doi.org/10.1021/acs.jpclett.3c01166
J. Phys. Chem. Lett. 2023, 14, 6071−6077

Similarly, we compute the mean distance between the P_{th} and P_{exp} values for state $\overline{\sigma}_{exp,j}$. The data are summarized in Table 1.

Table 1. Mean Distances of the State Populations Compared to the Ideal Theoretical Values for Photoexcitation and Electron-Transfer Processes

	photoexcitation		electron transfer	
	simulated time of 7.91 fs		simulated time of 32.91 fs	
	$\overline{\sigma}_{Tro}$	$\overline{\sigma}_{exp}$	$\overline{\sigma}_{Tro}$	$\overline{\sigma}_{exp}$
$\|D_1\rangle$	0.0067(18)	0.043(9)	0.024(3)	0.071(13)
$\|D_2\rangle$	0.0051(15)	0.044(9)	0.024(3)	0.078(13)
$\|A\rangle$	–	–	0.018(4)	0.043(9)

The $\overline{\sigma}_{Tro}$ of the electron-transfer process is larger than that of the photoexcitation process, as the error in the Trotter approximation reaches a larger value with a longer simulation time. To mitigate this effect, a larger number of Trotter steps N can be used to decrease the value of T/N in eq 13. However, due to experimental noise, the measured $\overline{\sigma}_{exp}$ is not dominated by the Trotter error. Improving the qutrit coherence time and accuracy of state preparation and measurements can reduce the experimental error. If experimental noise is no longer a dominant source of error, then increasing N needs to be considered.

In this study, we used a trapped-ion qutrit to simulate electron-transfer dynamics in a model molecular system as a function of driving light polarization. The use of a qutrit enables simulation of this three-level system dynamics using only single-qutrit operations on a single ion, whereas the use of conventional qubits would require multiple two-qubit operations on at least two ions. As a result, qutrit simulations exhibit enhanced simulation accuracy (see the Supporting Information for details). When simulations of larger systems comprising more than three states are conducted, the incorporation of entangling gates becomes necessary in the context of qutrits. Nonetheless, the number of entangling gates required for qutrits can be reduced compared to that for qubits.[18,19]

Through the qutrit simulation, we find that the photoexcitation process and the population difference for the two degenerate states are influenced by the exciting light polarization. We also studied the influence of phase differences between the two electron-transfer coupling pathways on the electron-transfer efficiency, finding that destructive interference occurs only when the energy level difference is very small ($\lesssim$0.73%). While the main focus of our study is on demonstrating the proof of principle, we believe it contributes significantly to the broader understanding of quantum dynamics in molecular systems, particularly in manipulating and controlling electron-transfer processes.[20] The mapping of this model onto a single qutrit with small gate errors offers an encouraging approach for simulating more complex quantum systems using trapped-ion qudits, potentially exceeding the current capabilities of classical digital computers.

Future research directions include simulating electron and excitation transfer in molecular systems with more complex connectivity, such as chemically linked donor–acceptor assemblies, which have a larger number of states. Such studies will likely require entangling operations on more than one ion, even with the use of qudits instead of qubits. The coherent control of trapped-ion qudits is a promising avenue for achieving more efficient and accurate simulations, potentially requiring fewer ions and entangling operations than qubits. However, two-qudit gates with higher fidelity are needed to conduct more complex simulations, as highlighted in recent studies.[13−16,21,22]

Another interesting future direction is to add interactions between the electronic states, and between these states and the surrounding environment.[8,17,23] For the PLET model, it is expected that the effects of light polarization will be diminished when interactions with the environment reduce the electronic coherence. To study this behavior, we can simulate PLET structures that have various interactions with the surrounding environment. The environment is often modeled as a bath of harmonic oscillators, which can be mapped to the normal modes of the motion of the trapped ions.[20,24] Indeed, a donor–acceptor system coupled to one or two harmonic oscillators has been simulated in recent experiments with trapped ions[9,25,26] and superconducting qubits coupled to electromagnetic cavities.[27]

EXPERIMENTAL METHODS

Experimental Setup. The simulation circuit is implemented on a $^{171}Yb^+$ ion confined in a microfabricated surface trap.[28] The qutrit energy levels are encoded as the hyperfine energy levels of the $^2S_{1/2}$ orbital: $|0\rangle \equiv |F = 0; m_F = 0\rangle$, $|1\rangle \equiv |F = 1; m_F = 0\rangle$, and $|2\rangle \equiv |F = 1; m_F = -1\rangle$. In this ion, the $|0\rangle$ and $|1\rangle$ states remain coherent and form an ideal qubit state. The coherence of $|2\rangle$ depends strongly on the ambient magnetic field noise. We use a mu-metal shield to reduce the magnetic field noise experienced by the atomic ion by >2 orders of magnitude, so all three qutrit states remain highly coherent.[29] The transitions from $|0\rangle$ to $|1\rangle$ and $|2\rangle$ are achieved using stimulated Raman transitions driven by a pair of laser beams.[30] We choose laser polarization settings so that the Rabi frequencies of $|0\rangle$ to $|1\rangle$ and $|0\rangle$ to $|2\rangle$ are close ($2\pi \times 17.30$ and $2\pi \times 17.49$ kHz, respectively). Acousto-optic modulators (AOMs) are used to tune the frequency and phase of each laser beam, while also allowing the beams to act as switches for each transition. At the end of the simulation, we have the ability to measure the probability of the qutrit in each of the states ($|0\rangle$, $|1\rangle$, and $|2\rangle$). In a standard qubit readout approach using a state-dependent fluorescence technique, the $|0\rangle$ state remains dark while both $|1\rangle$ and $|2\rangle$ states scatter photons (and therefore remain indistinguishable) upon illumination with the readout beam. To distinguish these two states, we first swap the population of the $|1\rangle$ ($|2\rangle$) state with the $|0\rangle$ state using their Raman transition (π-pulse) and then perform measurements of the dark state population to determine the probability of the qutrit state (prior to the swap) being in the $|1\rangle$ ($|2\rangle$) state. Details of the experimental setup are described in refs 29 and 30.

Trotterization and Trapped-Ion Operation. The Trotterization method provides a way to simulate the time evolution of a Hamiltonian with multiple noncommuting terms by simulating the unitary operation corresponding to each individual term for a short time duration and repeating this for each term and time step.[10,11] We use the Trotterization method to simulate the time evolution of $\hat{H}_1(t)$, which can be applied straightforwardly to $\hat{H}_2$. $\hat{H}_1(t)$ is written in the interaction picture as

$$\hat{H}_{I,1}(t) = \hat{H}^{(1)}_{I,1}(t) + \hat{H}^{(2)}_{I,1}(t) \tag{10}$$

where

https://doi.org/10.1021/acs.jpclett.3c01166
J. Phys. Chem. Lett. 2023, 14, 6071−6077

$$\hat{H}_{1,1}^{(1)}(t) = \mu_1 E_x(t) e^{i(\omega_G - \omega_{D_1})t} |G\rangle\langle D_1| + h.\,c. \tag{11}$$

$$\hat{H}_{1,1}^{(2)}(t) = \mu_2 E_y(t) e^{i(\omega_G - \omega_{D_2})t} |G\rangle\langle D_2| + h.\,c. \tag{12}$$

Time evolution $\hat{U}$ with respect to $\hat{H}_{1,1}(t)$ up to time T is Trotterized into N discrete time steps.

$$\hat{U} = \hat{U}_N \hat{U}_{N-1} \ldots \hat{U}_1 = \hat{U}_{ideal}(T) + O[(T/N)^3] \tag{13}$$

where

$$\hat{U}_{ideal}(T) = \mathcal{T} \exp\left[-i \int_0^T H_{1,1}(t')\, dt'\right] \tag{14}$$

where $\mathcal{T}$ is the time-ordering operator, which arranges the exponentiated Hamiltonians in the chronological order. Also, the time evolution for each time step is built from a second-order Trotter formula[11]

$$\hat{U}_j = e^{-i\hat{H}_{1,1}^{(1)}(t_j)T/2N} e^{-i\hat{H}_{1,1}^{(2)}(t_j)T/N} e^{-i\hat{H}_{1,1}^{(1)}(t_j)T/2N} \tag{15}$$

where $t_j \equiv (j - {}^1/_2)T/N$. Each step corresponds to a simulated time evolution of T/N, and we plot the dynamics according to this simulated time. N must be sufficiently large to simulate the time evolution of the system accurately.

We map molecular states $|G\rangle$, $|D_1\rangle$, and $|D_2\rangle$ to the trapped-ion qutrit states $|0\rangle$, $|1\rangle$, and $|2\rangle$, respectively. The evolution of the molecular states described above can be mapped to single-qutrit operations. For a transition between $|0\rangle$ and $|\alpha\rangle$ ($\alpha = 1$ or 2), the time evolution up to time $\tilde{\tau}$ is given by

$$\tilde{U} = e^{-i\tilde{H}\tilde{\tau}} \tag{16}$$

where

$$\tilde{H}_\alpha = \frac{\Omega_\alpha}{2} e^{i\phi_\alpha} |0\rangle\langle\alpha| + h.\,c. \tag{17}$$

where Ω_α and ϕ_α are the Rabi frequency and phase, respectively, determined by the intensity and phase of the laser beam that drives the transition. Thus, the values of amplitude $\mu_1 E_x(t_j)T/2N$ [$\mu_2 E_y(t_j)T/N$] and phase $(\omega_G - \omega_{D_1})$ t_j [$(\omega_G - \omega_{D_2})t_j$] of each term in eq 15 can be mapped to $\Omega_\alpha\tilde{\tau}$ and ϕ_α of the corresponding qutrit control operation, respectively. We can program these quantities by shaping the control laser beams.

In our experiments, it is desirable to use a fixed value of Ω_α because of the difficulty associated with calibrating and stabilizing the laser intensity that drives the transition between the atomic states. Thus, instead of tuning Ω_α, we vary the evolution time $\tilde{\tau}$ for each Trotterization step with a constant Rabi frequency Ω_α to simulate the electric field that varies over time. This method using Trotterization allows us to perform accurate simulations with a targeted upper bound on the error.

■ ASSOCIATED CONTENT

Supporting Information

The Supporting Information is available free of charge at https://pubs.acs.org/doi/10.1021/acs.jpclett.3c01166.

Hamiltonian for PLET simulation using a qubit system and a comparison of qubit simulation and qutrit simulation (PDF)

■ AUTHOR INFORMATION

Corresponding Authors

Ke Sun − *Duke Quantum Center, Duke University, Durham, North Carolina 27701, United States; Department of Physics, Duke University, Durham, North Carolina 27708, United States;* orcid.org/0000-0002-8311-9909; Email: ke.sun@duke.edu

Jungsang Kim − *Duke Quantum Center, Duke University, Durham, North Carolina 27701, United States; Department of Physics and Department of Electrical and Computer Engineering, Duke University, Durham, North Carolina 27708, United States; IonQ, Inc., College Park, Maryland 20740, United States*; Email: jungsang@duke.edu

Authors

Chao Fang − *Duke Quantum Center, Duke University, Durham, North Carolina 27701, United States; Department of Electrical and Computer Engineering, Duke University, Durham, North Carolina 27708, United States*

Mingyu Kang − *Duke Quantum Center, Duke University, Durham, North Carolina 27701, United States; Department of Physics, Duke University, Durham, North Carolina 27708, United States;* orcid.org/0000-0003-3032-8448

Zhendian Zhang − *Department of Chemistry, Duke University, Durham, North Carolina 27708, United States*

Peng Zhang − *Department of Chemistry, Duke University, Durham, North Carolina 27708, United States*

David N. Beratan − *Duke Quantum Center, Duke University, Durham, North Carolina 27701, United States; Department of Chemistry, Duke University, Durham, North Carolina 27708, United States; Department of Biochemistry, Duke University, Durham, North Carolina 27710, United States;* orcid.org/0000-0003-4758-8676

Kenneth R. Brown − *Duke Quantum Center, Duke University, Durham, North Carolina 27701, United States; Department of Physics, Department of Electrical and Computer Engineering, and Department of Chemistry, Duke University, Durham, North Carolina 27708, United States;* orcid.org/0000-0001-7716-1425

Complete contact information is available at: https://pubs.acs.org/10.1021/acs.jpclett.3c01166

Notes

The authors declare no competing financial interest.

■ ACKNOWLEDGMENTS

The authors express their gratitude to Ye Wang for his valuable contribution to the experimental setup. This research is funded by the Office of the Director of National Intelligence - Intelligence Advanced Research Projects Activity, through ARO Contract W911NF-16-1-0082, which provides support for the experimental apparatus utilized in J.K.'s laboratory, as well as by U.S. Department of Energy BES Awards DE-SC0019400 and DE-SC0019449, which support D.N.B.'s laboratory and J.K.'s laboratory, respectively, in terms of simulation methodology and analysis. In addition, the authors acknowledge the support of National Science Foundation Quantum Leap Challenge Institute for Robust Quantum Simulation Grant OMA-2120757, which supports the K.R.B.−J.K. joint laboratory's experimental implementation.

ADDITIONAL NOTE

[a]Whether this lower bound is achievable may depend on the structure and parameter values of the Hamiltonian. For example, ref 17 simulates a four-level system using two qubits, where the Hamiltonian parameters are chosen to obey certain symmetries.

REFERENCES

(1) Marcus, R. A. Chemical and Electrochemical Electron-Transfer Theory. *Annu. Rev. Phys. Chem.* **1964**, *15*, 155.
(2) Beratan, D. N. Why Are DNA and Protein Electron Transfer So Different? *Annu. Rev. Phys. Chem.* **2019**, *70*, 71.
(3) Prytkova, T. R.; Kurnikov, I. V.; Beratan, D. N. Coupling Coherence Distinguishes Structure Sensitivity in Protein Electron Transfer. *Science* **2007**, *315*, 622−625.
(4) Skourtis, S. S.; Beratan, D. N.; Naaman, R.; Nitzan, A.; Waldeck, D. H. Chiral Control of Electron Transmission Through Molecules. *Phys. Rev. Lett.* **2008**, *101*, 238103.
(5) Ray, K.; Ananthavel, S. P.; Waldeck, D. H.; Naaman, R. Asymmetric Scattering of Polarized Electrons by Organized Organic Films of Chiral Molecules. *Science* **1999**, *283*, 814−816.
(6) Yang, Y.; Da Costa, R. C.; Fuchter, M. J.; Campbell, A. J. Circularly Polarized Light Detection by a Chiral Organic Semiconductor Transistorecules. *Nat. Photon.* **2013**, *7*, 634−638.
(7) Feynman, R. P. *Feynman and computation*; CRC Press: Boca Raton, FL, 2018; pp 133−153.
(8) Maier, C.; Brydges, T.; Jurcevic, P.; Trautmann, N.; Hempel, C.; Lanyon, B. P.; Hauke, P.; Blatt, R.; Roos, C. F. Environment-Assisted Quantum Transport in a 10-qubit Network. *Phys. Rev. Lett.* **2019**, *122*, No. 050501.
(9) Gorman, D. J.; Hemmerling, B.; Megidish, E.; Moeller, S. A.; Schindler, P.; Sarovar, M.; Haeffner, H. Engineering Vibrationally Assisted Energy Transfer in a Trapped-Ion Quantum Simulator. *Phys. Rev. X* **2018**, *8*, No. 011038.
(10) Trotter, H. F. On the Product of Semi-Groups of Operators. *Proceedings of the American Mathematical Society* **1959**, *10*, 545−551.
(11) Suzuki, M. Generalized Trotter's Formula and Systematic Approximants of Exponential Operators and Inner Derivations With Applications to Many-Body Problems. *Commun. Math. Phys.* **1976**, *51*, 183−190.
(12) Hughes, R. J.; James, D. F. V.; Knill, E. H.; Laflamme, R.; Petschek, A. G. Decoherence Bounds on Quantum Computation With Trapped Ions. *Phys. Rev. Lett.* **1996**, *77*, 3240.
(13) Klimov, A. B.; Guzmán, R.; Retamal, J. C.; Saavedra, C. Qutrit Quantum Computer With Trapped Ions. *Phys. Rev. A* **2003**, *67*, No. 062313.
(14) Low, P.; White, B. M.; Cox, A. A.; Day, M. L.; Senko, C. Practical Trapped-Ion Protocols for Universal Qudit-Based Quantum Computing. *Phys. Rev. Res.* **2020**, *2*, No. 033128.
(15) Ringbauer, M.; Meth, M.; Postler, L.; Stricker, R.; Blatt, R.; Schindler, P.; Monz, T. A Universal Qudit Quantum Processor With Trapped Ions. *Nat. Phys.* **2022**, *18*, 1053−1057.
(16) Hrmo, P.; Wilhelm, B.; Gerster, L.; van Mourik, M. W.; Huber, M.; Blatt, R.; Schindler, P.; Monz, T.; Ringbauer, M. Native Qudit Entanglement in a Trapped Ion Quantum Processor. *Nat. Commun.* **2023**, *14*, 2242.
(17) Wang, B.; Tao, M.; Ai, Q.; Xin, T.; Lambert, N.; Ruan, D.; Cheng, Y.; Nori, F.; Deng, F.; Long, G. Efficient Quantum Simulation of Photosynthetic Light Harvesting. *npj Quantum Information* **2018**, *4*, 52.
(18) Brylinski, J.; Brylinski, R. *Mathematics of quantum computation*; Chapman and Hall/CRC: 2002; pp 117−134.
(19) Gokhale, P.; Baker, J. M.; Duckering, C.; Brown, N. C.; Brown, K. R.; Chong, F. T. Asymptotic Improvements to Quantum Circuits via Qutrits. Proceedings of the 46th International Symposium on Computer Architecture. 2019; pp 554−566.
(20) Schlawin, F.; Gessner, M.; Buchleitner, A.; Schätz, T.; Skourtis, S. S. Continuously Parametrized Quantum Simulation of Molecular Electron-Transfer Reactions. *PRX Quantum* **2021**, *2*, No. 010314.
(21) Chi, Y.; Huang, J.; Zhang, Z.; Mao, J.; Zhou, Z.; Chen, X.; Zhai, C.; Bao, J.; Dai, T.; Yuan, H.; et al. A Programmable Qudit-Based Quantum Processor. *Nat. Commun.* **2022**, *13*, 1166.
(22) Cervera-Lierta, A.; Krenn, M.; Aspuru-Guzik, A.; Galda, A. Experimental High-Dimensional Greenberger-Horne-Zeilinger Entanglement With Superconducting Transmon Qutrits. *Phys. Rev. Appl.* **2022**, *17*, No. 024062.
(23) Potočnik, A.; Bargerbos, A.; Schröder, F. A. Y. N.; Khan, S. A.; Collodo, M. C.; Gasparinetti, S.; Salathé, Y.; Creatore, C.; Eichler, C.; Türeci, H. E.; Chin, A. W.; Wallraff, A. Studying Light-Harvesting Models With Superconducting Circuits. *Nat. Commun.* **2018**, *9*, 904.
(24) MacDonell, R. J.; Dickerson, C. E.; Birch, C. J. T.; Kumar, A.; Edmunds, C. L.; Biercuk, M. J.; Hempel, C.; Kassal, I. Analog Quantum Simulation of Chemical Dynamics. *Chem. Sci.* **2021**, *12*, 9794−9805.
(25) Whitlow, J.; Jia, Z.; Wang, Y.; Fang, C.; Kim, J.; Brown, K. R. Simulating Conical Intersections With Trapped Ions. *arXiv* **2022**, DOI: 10.48550/arXiv.2211.07319.
(26) Valahu, C. H.; Olaya-Agudelo, V. C.; MacDonell, R. J.; Navickas, T.; Rao, A. D.; Millican, M. J.; Pérez-Sánchez, J. B.; Yuen-Zhou, J.; Biercuk, M. J.; Hempel, C. Direct Observation of Geometric Phase in Dynamics Around a Conical Intersection. *arXiv* **2022**, DOI: 10.48550/arXiv.2211.07320.
(27) Wang, C. S.; Frattini, N. E.; Chapman, B. J.; Puri, S.; Girvin, S. M.; Devoret, M. H.; Schoelkopf, R. J. Observation of Wave-Packet Branching Through an Engineered Conical Intersection. *Phys. Rev. X.* **2023**, *13*, No. 011008.
(28) Revelle, M. C. Phoenix and Peregrine Ion Traps. *arXiv* **2020**, DOI: 10.48550/arXiv.2009.02398.
(29) Fang, C.; Wang, Y.; Sun, K.; Kim, J. Realization of Scalable Cirac-Zoller Multi-Qubit Gates. *arXiv* **2023**, DOI: 10.48550/arXiv.2301.07564.
(30) Wang, Y.; Crain, S.; Fang, C.; Zhang, B.; Huang, S.; Liang, Q.; Leung, P. H.; Brown, K. R.; Kim, J. High-Fidelity Two-Qubit Gates Using a Microelectromechanical-System-Based Beam Steering System for Individual Qubit Addressing. *Phys. Rev. Lett.* **2020**, *125*, 150505.

https://doi.org/10.1021/acs.jpclett.3c01166
J. Phys. Chem. Lett. 2023, 14, 6071−6077